JOURNAL OF Materials CHEMISTRY

Structure, morphology and surface properties of nanostructured ZrO_2 particles

Sigrid Benfer† and Erich Knözinger*

Institut für Physikalische Chemie, TU Wien, Getreidemarkt 9/156, A-1060 Wien, Austria. Fax: 0043-1-58801-15699. E-mail: knoezinger@buwien.ac.at

Received 24th November 1998, Accepted 18th February 1999

Nanocrystalline zirconium dioxide particles have been produced by means of thermal decomposition of a liquid metal organic precursor in a flow reactor system. X-Ray diffraction patterns show that the powder consists of a mixture of the monoclinic and tetragonal phase and that the phase fractions depend on the experimental conditions during the preparation as well as on the subsequent thermal treatment of the sample. The mean particle diameter of the synthesized powders is *ca.* 40–50 Å as estimated from the line width of Bragg reflections and from transmission electron micrographs. The crystallites are non-porous and exhibit a rough surface incorporating a high concentration of low-coordinated surface sites. In agreement with the small particle size, the powder has a high specific surface area ($>200\ m^2\ g^{-1}$), which surmounts that of commercially available materials by a factor >3. The structure and morphology of the particles is essentially preserved during extensive thermal treatment up to 500 °C. Hydroxyl groups as IR active surface probes clearly indicate that the phase fractions on the surface and in the bulk strongly differ from each other.

Low-coordinated OH groups on monoclinic surface domains give rise to H/D exchange reactions with D_2 already at room temperature. They are evidenced and monitored with time by FTIR spectroscopy.

Introduction

For various reasons zirconium dioxide has met an increasing interest in heterogenous catalysis. Adsorption studies of CO_2 and NH_3 clearly show that ZrO_2 surfaces exhibit both acidic and basic centres.[1] Its high melting point and stability under reducing conditions favours applications of ZrO_2 as a support material for catalytically active species. It is, however, also catalytically active itself. Examples are the hydrogenation of CO,[2] olefins[3] and dienes.[4]

The application of zirconium dioxide as a catalyst or as a catalyst support necessarily implies the presence of a high specific surface area which is retained under process conditions. Various methods aiming at the production of nanometer-sized ZrO_2 have been described in the literature.[5–9] The reduced particle size not only guarantees an increased specific surface area (quantitative change of surface reactivity) but also raises the fraction of low-coordinated surface sites (qualitative change of surface reactivity).

At room temperature the thermodynamically stable phase of ZrO_2 is monoclinic. High temperature phases, in particular the tetragonal phase may be stabilized by the addition of carefully selected impurities such as Y_2O_3[10] or frozen out by applying non-equilibrium techniques during the production process.[11] All attempts aiming at the reduction of particle dimensions down to the nanometer domain also necessarily rely upon non-equilibrium conditions of production. Thus the tetragonal phase should play a more dominating role in these small particles. The situation is, however, more complicated. The specific surface energies of tetragonal and monoclinic ZrO_2 are significantly different. The stability criteria are, therefore, different for nanometer-sized and equilibrium ZrO_2. Consequently the objective of the present study, which is to shed light on the chemical properties of reactive surface sites of ZrO_2, must include a careful surface phase analysis of nanometer-sized ZrO_2 particles.

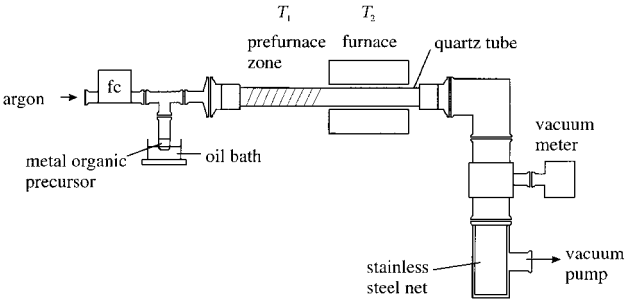

Fig. 1 Schematic representation of the flow reactor system for the production of nanostructured ZrO_2; fc: flow controller; T_1, T_2: temperature of the pre-furnace zone and the furnace, respectively.

Experimental

Synthesis of nanostructured ZrO_2 particles

Nanostructured ZrO_2 particles (CVD ZrO_2) are prepared by the decomposition of zirconium *tert*-butoxide (99.99%, Heraeus) in a flow reactor system (Fig. 1). The liquid metal organic precursor is evaporated at temperatures in the range 110–135 °C at a reduced pressure of 5–20 mbar. Ar is used as the diluting agent and carrier gas which transports the evaporated molecules to the furnace zone. In this area the metal oxide particles are formed by the decomposition of the precursor molecules. They are then deposited downstream in a stainless steel net. The raw material is cleaned from adsorbed hydrocarbons by an annealing and oxygen treatment at 500 °C.

Instrumentation

For the X-ray diffraction experiments a powder diffractometer (type XRD 3000 TT, Seifert) providing monochromatic Cu-Kα_1 radiation was applied. The adsorption measurements to calculate specific surface area were performed according to the BET method.[12] High resolution electron microscopy (HREM) images were recorded on a Philips CM 12 at the Hahn-Meitner-Institut (HMI, Berlin) using a CCD camera. The IR

†Current address: TU Bergakademie Freiberg, Institut für Keramische Werkstoffe, Gustav-Zeuner-Straße 3, D-09596 Freiberg, Germany.

spectra were recorded on a FTIR spectrometer (model IFS 113v, Bruker Analytisch Meßtechnik GmbH) using a liquid-N_2-cooled MCT for the mid-IR (4000–500 cm^{-1}) region. The applied resolution was 1 cm^{-1}. A reasonable S/N could be guaranteed by averaging 100 interferograms.

Sample preparation

For the IR studies the powders were pressed into thin self-supporting disks of *ca.* 10–15 mg cm^{-2}. These disks were then introduced into the IR transmission cell decribed elsewhere.[13]

Reference materials

Commercially available ZrO_2 powders (ZrO_2/2094E and ZrO_2/Et57) provided by Degussa were used as reference materials. They were synthesized by flame hydrolysis from $ZrCl_4$.

Processing of the XRD data

The X-ray diffractograms were fitted by a Rietveld refinement to determine the phase composition and mean diameter of the particles. Using the equations from Scherrer[14,15] and Caglioti *et al.*[16] the particle size can be estimated from the profile function. The phase composition results directly from the refinement.

Results

Properly selected thermal treatment of highly dispersed materials such as metal oxides in general initiates particle growth and changes of the surface structure. These effects are known as sintering. Polymorphic materials, such as ZrO_2, furthermore exhibit structural changes of the bulk during thermal treatment. They originate from changes in the phase composition and clearly influence, even though indirectly, the local surface structure.

In order to obtain detailed information on thermally induced variations of both bulk structure and particle morphology of the nanostructured ZrO_2, XRD, TEM and BET measurements were carried out. On the other hand isolated OH groups were monitored as IR active probes for the local surface structure and its thermally induced changes. For systematic studies the ZrO_2 samples under investigation were, independent of the analysis technique applied, subjected to a standardized program of thermal treatment: 500, 600, 700, and 800 °C for 30 min. Any differences, if required, will be indicated separately.

(a) Structure and morphology (XRD, BET and TEM results)

X-Ray diffraction patterns of the gas phase deposited ZrO_2 material show broad Bragg reflections (Fig. 2) indicating the presence of small crystallites with a mean diameter of <50 Å (500 °C). The crystallite size increases with increasing pretreatment temperature because of sintering (Table 1). After thermal treatment at 600 °C the respective mean crystallite diameter obtained by XRD is <60 Å and provides a specific surface area which is in good agreement with BET data. The presence of porosity may, therefore, be excluded (Table 1). On the other hand, the temperature increase from 500 to 600 °C gives rise to a decrease of the monoclinic phase fraction (Table 1). This tendency is completely reversed at temperatures between 600 and 800 °C which initiate extensive sintering also evidenced by BET measurements (Table 1).

The commercially available ZrO_2(2094E, Degussa AG Hanau), produced by flame hydrolysis, exhibits a much higher tetragonal phase fraction than the CVD material and consists of significantly larger particles (Fig. 2, Table 1). On raising the temperature of treatment from 500 to 800 °C both the monoclinic phase fraction and the particle size monotonously increase (Table 1).

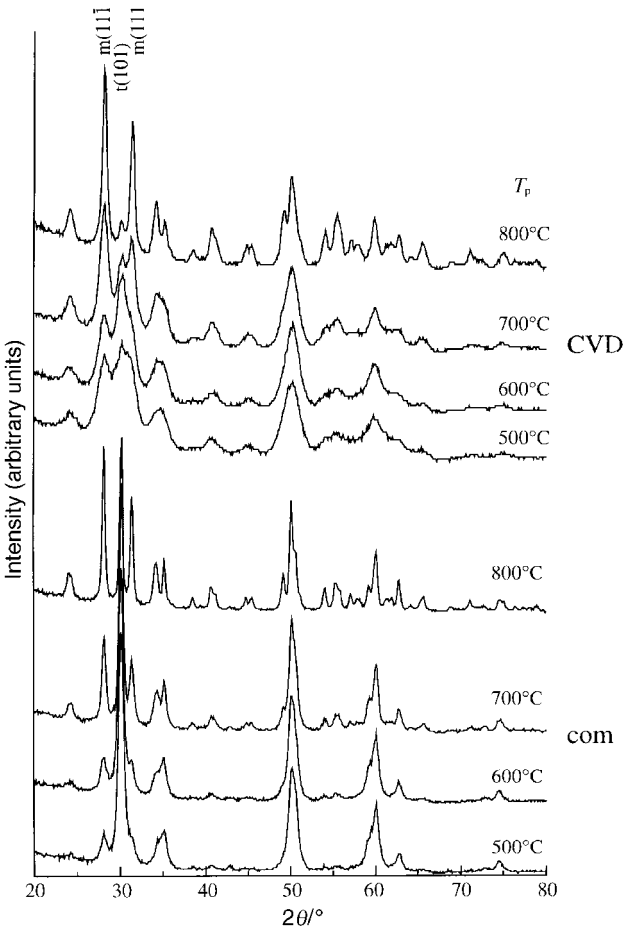

Fig. 2 X-Ray diffraction pattern of CVD ZrO_2 and commercial ZrO_2 (2094E) pretreated at different temperatures; time of pretreatment: 30 min; m: monoclinic, t: tetragonal, com: commercial.

Fig. 3a shows the specific surface area of the CVD material as a function of both temperature and time of pretreatment. The value of 230 $m^2 g^{-1}$ is preserved up to 500 °C. The sintering effects observed during pretreatment at higher temperatures lead to a specific surface area comparable to that of the commercial material without any thermal treatment (Fig. 3b).

High resolution TEM studies of the CVD ZrO_2 show small crystallites with a rough surface (Fig. 4a). The interference patterns of the crystal lattice planes are well resolved and defects are not detectable. The interplanar spacing observed ($d=3.139$ Å) is in good agreement with the value for the (11$\bar{1}$)-planes of the monoclinic structure. More than one hundred particles were measured to estimate the particle size distribution of the CVD ZrO_2 powder. The experimental values can be fitted with a log–normal function. The material treated

Table 1 Monoclinic phase fraction (X_m), crystallite sizes (D_m, D_t) of monoclinic and tetragonal crystallites, respectively, and specific surface area determined by XRD (O_{XRD}) and BET (O_{BET}) of CVD and commercial ZrO_2 subjected to varying pretreatment temperatures (T_p)

Material	T_p/ °C	X_m(%)	D_m/ Å	$O_{XRD,m}$/ $m^2 g^{-1}$	D_t/ Å	$O_{XRD,t}$/ $m^2 g^{-1}$	O_{BET}/ $m^2 g^{-1}$
CVD	500	58.0	48	224	39	273	218
	600	54.5	57	189	53	201	201
	700	83.0	75	152	66	162	145
	800	92.1	129	83	113	95	80
com	500	14.8	99	108	111	96	87
	600	24.0	115	93	114	94	85
	700	43.3	154	70	154	70	68
	800	66.9	219	49	221	48	31

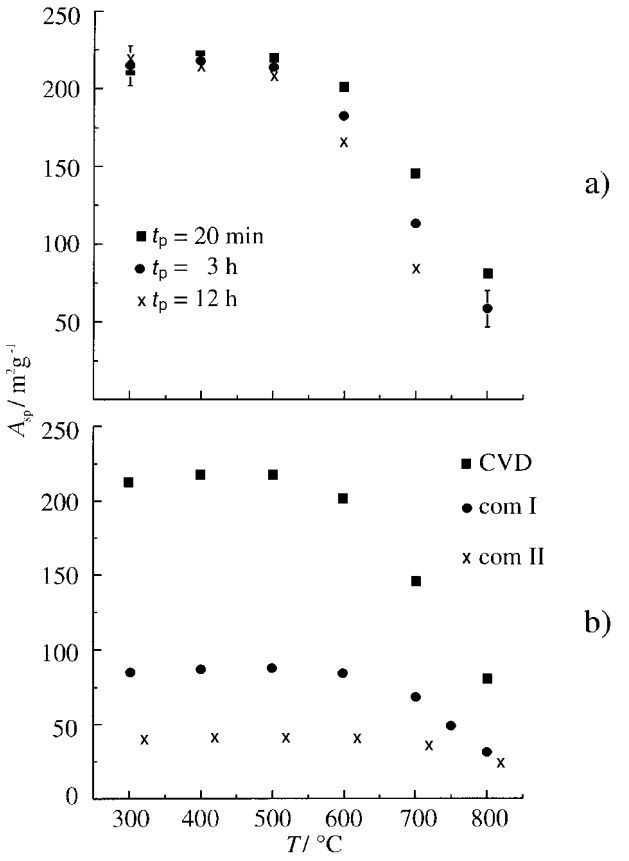

Fig. 3 a) Specific surface area of CVD ZrO_2 as a function of temperature and time of pretreatment; b) specific surface area of different ZrO_2 materials (com I: 2094E, com II: Et57) as a function of pretreatment.

at 500 °C exhibits a very small distribution ($\sigma = 1.3$) with a mean diameter of 46 Å (Fig. 5). Thermal treatment at 800 °C for 3 h leads to a considerable increase of the particle size (219 Å) and broadening of the distribution function ($\sigma = 1.4$) (Fig. 5). Transmission electron micrographs show that the particles now exhibit more regular planes on their surfaces (Fig. 4b).

(b) Local surface structure (IR spectroscopic investigations)

The standardized procedure of creating isolated OH groups which are used as IR active surface probes comprises hydroxylation at room temperature and subsequent degassing for 20 min at 500 °C. Prior to this procedure, the ZrO_2 sample was thermally treated at temperatures in the range 500–800 °C, as mentioned above.

Independent of the type of thermal pretreatment the IR spectra of CVD ZrO_2 with isolated OH groups attached to the surface exhibit two clearly separated stretching bands centred around 3770 and 3670 cm^{-1} which will be designated as $(OH)_I$ and $(OH)_{II}$, respectively (Fig. 6). Their contour sensitively depends on the thermal pretreatment applied and, therefore, reflects the distribution of surface OH groups as well as any relevant changes. With increasing pretreatment temperature the band intensity in the low frequency range of both bands $(OH)_I$ and $(OH)_{II}$ (3760 and 3650 cm^{-1}) decreases significantly. A new band at 3690 cm^{-1} appears in the high frequency range of the band $(OH)_{II}$.

The above introduced surface OH groups exhibit site selective reactivity with respect to D_2 at room temperature. This is shown for a CVD sample thermally pretreated at 500 °C. During the reaction with D_2 both OH stretching bands lose intensity mainly in the low frequency range (Fig. 7). At

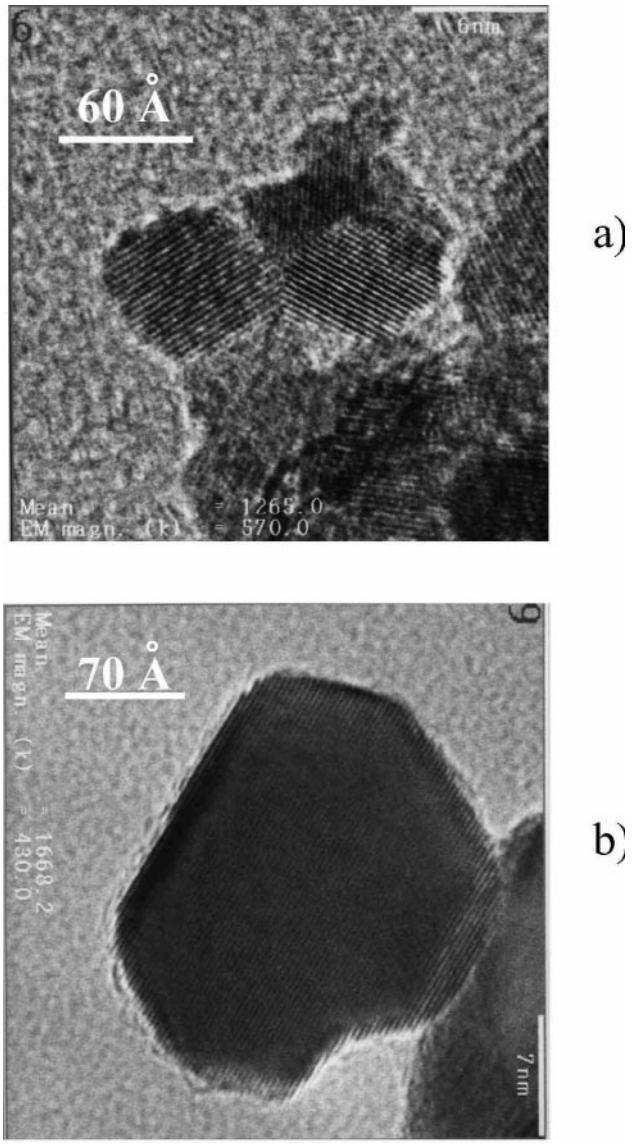

Fig. 4 High resolution transmission electron micrographs of CVD ZrO_2 thermally treated at 500 °C (a, magnification: 570,000) and 3 h at 800 °C (b, magnification: 430,000).

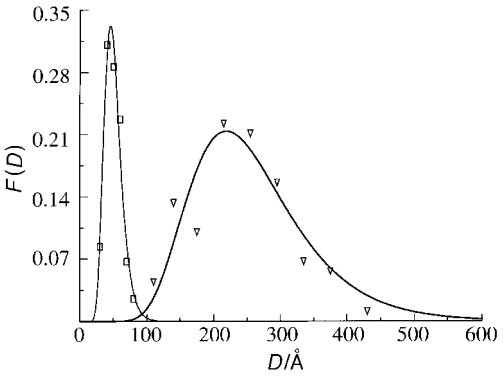

Fig. 5 Crystallite size distribution $F(D)$ derived from TEM images of CVD ZrO_2; pretreatment temperatures: 500 °C (□) and 800 °C (▽).

the same time an intensity increase in the OD stretching region is observed as shown by IR difference spectra (Fig. 7b). Owing to the site selectivity of the H/D exchange the half width of the difference bands (Fig. 7b) is significantly smaller than that of the original bands representing the complete distribution of OH groups (Fig. 7a).

Equally pretreated commercial ZrO_2 samples (2094E) do

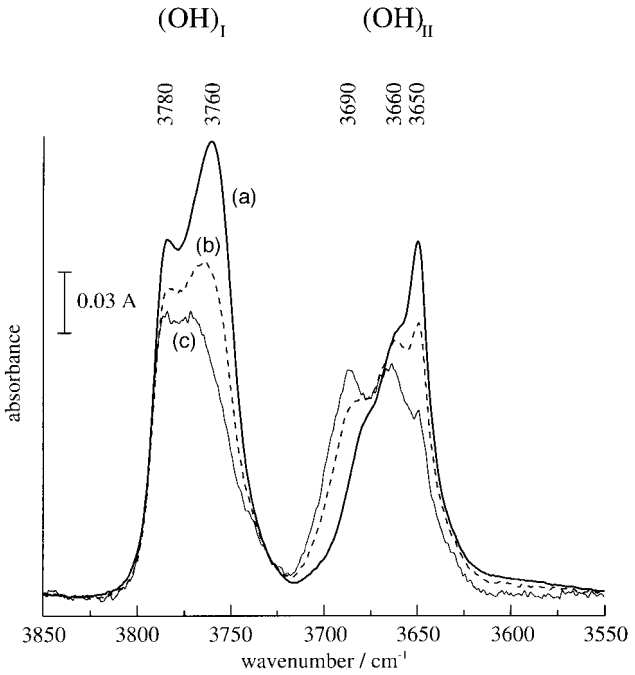

Fig. 6 IR spectra of isolated OH groups on CVD ZrO_2 after degassing at 500 °C; thermal pretreatment at $T_p = 500$ (a), 700 (b) and 800 °C (c).

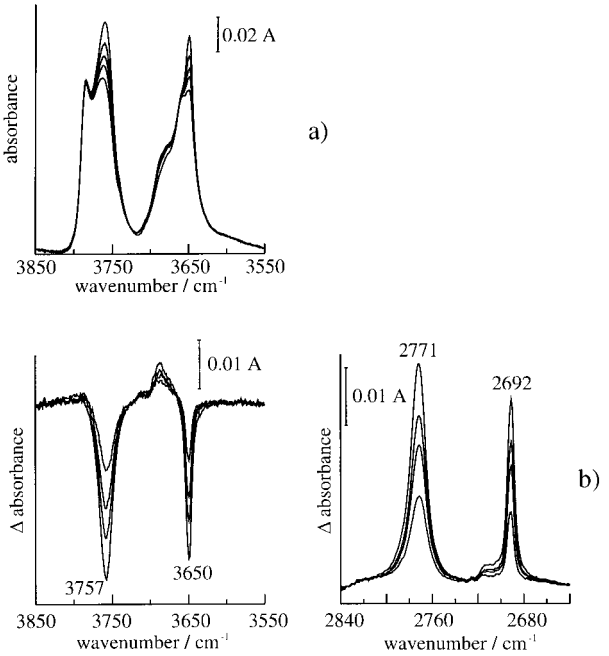

Fig. 7 IR spectra of isolated OH groups on CVD ZrO_2 during the reaction with D_2 gas at room temperature (pretreatment and degassing temperature: 500 °C); a) original spectra of the OH stretching region, b) difference spectra obtained by subtracting the absorbance spectra before from those after the D_2 admission.

not react with D_2 under the same conditions as applied to the CVD samples (Fig. 8). Obviously the CVD procedure creates reactive surface sites which are not available on the material produced by flame hydrolysis.

Discussion

(a) Structure and morphology

Zirconium dioxide exists in different modifications, namely monoclinic, tetragonal and cubic. Under normal conditions the thermodynamically stable phase is the monoclinic one.

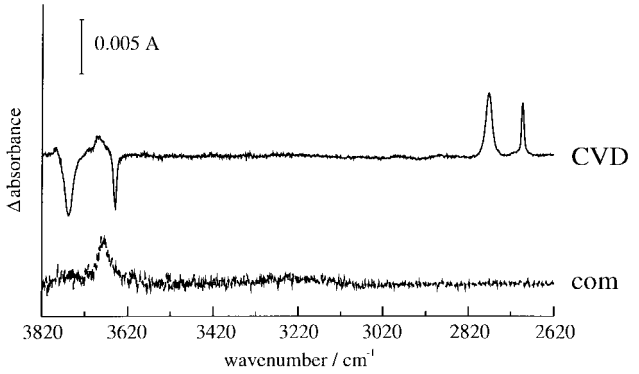

Fig. 8 IR difference spectra (see legend of Fig. 7b) for the H/D isotope exchange at room temperature (1 h, 120 mbar D_2) for two different ZrO_2 samples pretreated and degassed equally at 500 °C (the spectra are normalized to the same surface area).

Both high temperature modifications can be stabilized at room temperature by the addition of low valence cations, *e.g.* Y^{3+} or Ca^{2+}. The resulting phase composition depends on the amount of the dopant.[10,17] A metastable tetragonal phase may be present in pure zirconium dioxide, provided non-equilibrium techniques of production are applied which, in general, lead to a high surface area material. Under these circumstances differences in the specific surface energies of monoclinic and tetragonal ZrO_2 may become the dominating parameter in the stability criteria. In a single crystal the monoclinic structure has significantly less energy (bulk energy) than the tetragonal structure. Therefore, the thermodynamically stable phase at equilibrium conditions is the monoclinic one. On the other hand the specific surface energy of the tetragonal phase is considerably lower than that of the monoclinic phase.[18] If the crystallite size is reduced the contribution of the surface energy to the total energy increases. Thus below a characteristic critical crystallite size the tetragonal phase should be more stable than the monoclinic phase. This critical crystallite size depends on the temperature.[19] A value of *ca.* 100 Å was estimated by Garvie[20] at room temperature. These predictions neglect strain originating from lattice defects as well as adsorption of impurities on the surface. Furthermore the specific surface energy is assumed to be independent of the crystallite size. For nanometer-sized particles this is certainly not true.

The nanostructured ZrO_2 material obtained by CVD exhibits a mean particle diameter of 40–50 Å. The theoretical predictions, therefore, clearly favour the tetragonal phase as being the more stable.[20] X-Ray diffraction provides, however, clear evidence for the coexistence of monoclinic and tetragonal phases at room temperature (Fig. 2). The presence of the monoclinic phase may be explained by the synthesis procedure. Chemical vapour deposition leads to the production of non-equilibrium solids. Therefore, the monoclinic phase is frozen out in small particles. The observed decrease of the monoclinic phase fraction caused by thermal treatment at 600 °C (Table 1) may then be explained as follows: the input of thermal energy initiates the transformation of the monoclinic into the tetragonal phase which owing to the crystallite size effect is the 'equilibrium' structure. Thermal treatment at higher temperatures leads to extensive sintering of the material. The mean particle diameter increases and finally exceeds the critical value. The tetragonal phase then should no longer be stabilized and, consequently, an increase of the monoclinic phase fraction is observed (Table 1).

Compared to the CVD material, equally pretreated commercial ZrO_2 always, independent of the pretreatment temperature applied, exhibits a higher tetragonal phase fraction (Fig. 2, Table 1), although the mean particle diameter of the commercial ZrO_2 is greater by a factor of at least two. Therefore, the stabilization of the metastable tetragonal phase

in the commercial material cannot be explained by crystallite size effects. More likely is a stabilization by impurities[10,17] such as Cl^- anions originating from flame hydrolysis of $ZrCl_4$. On raising the pretreatment temperature a continuous increase of the monoclinic phase fraction is observed (Fig. 2). Sintering of the particles and reduction of impurity (Cl^-) concentration by the thermal pretreatment in vacuum may explain this behaviour.

The mean particle diameter of the CVD ZrO_2 was estimated from the broadening of the Bragg reflections. For samples treated at 500 °C a value of 48 Å was derived which is in good agreement with the data obtained from transmission electron micrographs. Obviously strain and lattice defects which contribute to the half width of Bragg reflections[15,21] do not play an important role here. This conclusion is confirmed by high resolution electron micrographs (Fig. 4). Defects inside the crystallites are not detectable to any significant extent. However, the small, nearly spherical particles exhibit irregular surface structures (Fig. 4a) and they are not confined by extended regular crystal planes. Therefore, the material should contain a high concentration of low-coordinated surface centres which would necessarily imply an enhanced surface reactivity. EXAFS measurements show that the mean coordination number of the zirconium atoms is reduced in nanocrystalline ZrO_2 ($D=300$ Å) compared to powders with much larger particles ($D=10000$ Å).[22] Thermal pretreatment at high temperatures (3 h, 800 °C) leads to a considerable increase of the mean particle diameter of the CVD material (Fig. 5). The crystallite growth is accompanied by significant changes of the surface structure. After the thermal pretreatment the dominating building elements of the surface show more extended regular planes (Fig. 4b). This means a reduction of the fraction of low-coordinated and highly reactive surface sites.

The specific surface areas estimated from XRD patterns *via* the mean particle diameters are also in good agreement with corresponding BET data (Table 1). Porosity of the CVD ZrO_2 material may, therefore, be excluded. For highly sintered samples the BET values are smaller than the values determined from XRD. This may be interpreted in terms of grain boundaries which are not accessible for BET probes (N_2). The CVD ZrO_2 exhibits a constant specific surface area of >200 m^2 g^{-1} up to 500 °C. Although sintering at higher pretreatment temperatures leads to a significant loss of specific surface area, CVD ZrO_2 preserves a value which is comparable to that of the commercial materials without any thermal treatment (Fig. 3).

(b) Local surface structure

The IR spectra of isolated OH groups on pure ZrO_2 phases exhibit one or two structured bands (Table 3). For CVD ZrO_2 (no additives) two bands are always observed. Their intensity ratio and their intensity distribution within each of the bands are unequivocally related to the surface phase composition and the local surface structure, respectively (Table 3). The detailed discussion of the parameters mentioned above will lead to assignments of different parts of the OH stretching bands to defined centres and phases of the surface.

Number of different oxygen species. In agreement with the existence of trigonally and tetrahedrally coordinated O^{2-} anions in the monoclinic lattice[23,24] there are two different types of O^{2-} anions in the surface which also induce two different surface sites of Zr^{4+} cations.[25] In the tetragonal lattice, on the other hand, only tetrahedrally coordinated O^{2-} anions exist.[26] Correspondingly there is only one type of O^{2-} anion and one type of Zr^{4+} cation in the surface.[25] Consequently the chemisorption of water on facets of monoclinic ZrO_2 and subsequent thermal pretreatment at 500 °C (*in vacuo*) lead to two families of isolated surface OH groups.

Table 2 Intensity ratio of the bands $(OH)_I$ and $(OH)_{II}$ for CVD ZrO_2 pretreated at different temperatures

Material	T_p/ °C	$A(OH)_I/A(OH)_{II}$
CVD	500	1.394
	600	1.267
	700	1.088
	800	1.007

Each family consists of one-coordinated (O from H_2O) and multiply coordinated (O from ZrO_2) OH groups. The same procedure applied to tetragonal ZrO_2 induces the formation of only one family of isolated OH groups. The two pure ZrO_2 phases both exhibit the band $(OH)_{II}$ centred around 3670 cm^{-1} which must, therefore, be related to the tetrahedrally coordinated bulk oxygen which is present in monoclinic and tetragonal ZrO_2. The band $(OH)_I$, on the other hand, is exclusively observed for monoclinic ZrO_2[25] which, differently from tetragonal ZrO_2, contains also trigonally coordinated bulk oxygen.

Phase composition in the surface. On the basis of the assignment above, changes in the phase composition of the zirconium oxide surface can be monitored by changes of the ratio of the integral intensities $A(OH)_I/A(OH)_{II}$. Table 2 contains the respective data for the CVD ZrO_2. With increasing pretreatment temperature a continuous decrease of the ratio $A(OH)_I/A(OH)_{II}$ is observed which reflects a decrease of monoclinic surface domains with respect to tetragonal ones. The tetragonal modification exhibits a smaller surface energy than the monoclinic one[18] and, therefore, the tetragonal phase will be stabilized at the surface of ZrO_2 particles. The synthesis of nanometer-sized ZrO_2 by CVD seems to favour the formation of a monoclinic surface phase which is frozen out by rapid cooling during the production process. Thermal treatment of the sample then induces a phase change from the monoclinic to the tetragonal phase at the surface, although an increase of the monoclinic phase is observed in the bulk (Table 1). Simultaneously with the decrease of the ratio $A(OH)_I/A(OH)_{II}$ both bands lose relative intensity in the low frequency range, whereas the high frequency component (3690 cm^{-1}) of the band $(OH)_{II}$ is increased in relative intensity (Fig. 6). OH groups which contribute to the absorption of the band $(OH)_I$ are located on monoclinic surface domains.[25] The simultaneous intensity decrease of $(OH)_I$ and of the sub-bound of $(OH)_{II}$ at 3650 cm^{-1} leads to the conclusion that this part of $(OH)_{II}$ may also be attributed to OH groups attached to monoclinic surface domains (Fig. 9). As mentioned above, a more extensive sample pretreatment favours the tetragonal surface phase. Therefore, the high frequency range of the band $(OH)_{II}$ (3690 cm^{-1}) which is increased in intensity during the pretreatment is attributed to OH groups on tetragonal surface domains (Fig. 9).

Table 3 Particle surface properties and their influence on the IR spectrum of isolated OH groups (OH stretching region)

Surface property of the particles		Characteristic features in the IR spectrum
Pure phase		
Tetragonal		1 OH band [$(OH)_{II}$]
Monoclinic		2 OH bands [$(OH)_I$ and $(OH)_{II}$]
Mixed phase		2 OH bands [$(OH)_I$ and $(OH)_{II}$]
Phase composition	↔	Ratio of band intensities $A(OH)_I/A(OH)_{II}$
Local structure (coordination, bond distances)	↔	Intensity distribution within each of the two bands $(OH)_I$ and $(OH)_{II}$

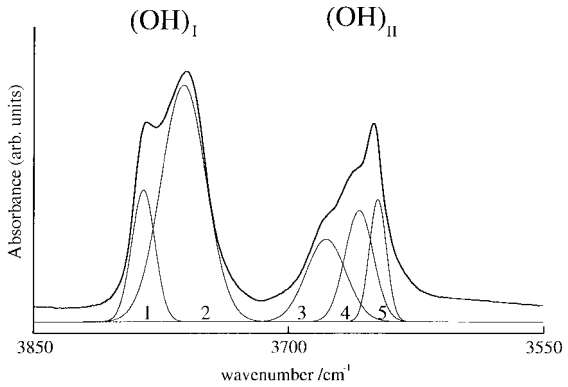

Band type	Band no.	Phase	OH species
$(OH)_I$	1	m	Zr^{4+}–OH
	2	m	O^{2-}–H
$(OH)_{II}$	3	t	Zr^{4+}–OH
	4	t	O^{2-}–H
		m	Zr^{4+}–OH
	5	m	O^{2-}–H

Fig. 9 Model for the assignment of different surface OH species to particular components of the bands $(OH)_I$ and $(OH)_{II}$; m: monoclinic; t: tetragonal; Zr^{4+}–OH: OH group with O from H_2O; O^{2-}–H: OH group with O from ZrO_2 bulk.

Local structure. As mentioned above the chemisorption of water leads to the formation of one-coordinate OH groups (O from H_2O) and multiply coordinated OH groups (O from ZrO_2). The contour of both OH stretching bands is, therefore, influenced by the ratio of these two types of surface OH groups. As in the case of MgO,[27] the one-coordinate OH groups give rise to the high frequency part of the OH stretching bands and the multiply coordinated OH groups to the low frequency part.[25] Thus the changes in the IR spectrum of surface OH groups on CVD ZrO_2 with increasing pretreatment temperature (Fig. 6) reflect differences in the thermal stability of (a) monoclinic and tetragonal surface domains (as discussed above) and (b) the relative amount of one-coordinate OH groups on surface Zr^{4+} cations and OH groups which incorporate a low-coordinated O^{2-} anion of the ZrO_2 surface. A comparison of the transmission electron micrographs of differently thermally treated CVD ZrO_2 samples shows how the surface morphology changes during the pretreatment procedure (Fig. 4). The crystallites exhibit much more regular planes on their surfaces after thermal treatment at 800 °C (Fig. 4b) as compared to 500 °C (Fig. 4a). The development of smooth surfaces is likely accompanied by the reduction of the amount of low-coordinated surface centres. These changes in surface morphology, observed by TEM, should also be reflected in the IR spectra of surface OH groups. OH groups which give rise to the band $(OH)_I$ are associated with, in the bulk, trigonally coordinated O^{2-} anions of the monoclinic structure. On the surface of the oxide the coordination of the anions and cations is necessarily reduced compared to the bulk. Therefore, the surface may exhibit two- and also one-coordinate O^{2-} anions and the latter should be concentrated on non-regular domains of the surface. With increasing temperature of thermal pretreatment the amount of low-coordinated surface centres should be reduced. The observed intensity decrease at 3760 cm^{-1} (Fig. 6, band no. 2 in Fig. 9) leads to the conclusion that this part of the band $(OH)_I$ originates from low-coordinated OH groups (O from ZrO_2). The band centred around 3780 cm^{-1} (band no. 1 in Fig. 9) must then be attributed to one-coordinate OH groups (O from H_2O) on low-coordinated Zr^{4+}. Obviously, the Zr^{4+} surface centres are thermally more stable than the O^{2-} surface sites. The observed intensity decrease at 3780 cm^{-1} is significantly smaller than that at 3760 cm^{-1} (Fig. 6). The tetrahedrally coordinated O^{2-} anions in the bulk [band $(OH)_{II}$] which exist in the monoclinic and tetragonal structure give rise to three- and two-coordinate surface O^{2-} anions. Also in this case thermal pretreatment should reduce the number of low-coordinated surface sites (band no. 5 in Fig. 9). The intensity decrease at 3650 cm^{-1} is reinforced by the simultaneous phase transformation at the surface from the monoclinic to the tetragonal phase. The band intensity at 3660 cm^{-1} which seems to be unaffected by thermal pretreatment (Fig. 6, band no. 4 in Fig. 9) then results from the superposition of two effects, namely the loss of low-coordinated Zr^{4+} centres on monoclinic surface domains and the simultaneous increase of low-coordinated O^{2-} centres on tetragonal surface domains. Finally, the band at 3690 cm^{-1} (Fig. 6, band no. 3 in Fig. 9) results from the increasing concentration of low-coordinated Zr^{4+} centres related to tetragonal surface structures.

According to specific environment potentials of the surface OH groups these exhibit different degrees of reactivity with respect to D_2 in the gas phase. Significant H/D isotope exchange on CVD ZrO_2 (pretreated at 500 °C) already at room temperature is detected by FTIR spectroscopy (Fig. 7). The process is clearly site selective: the OH groups giving rise to the low-frequency part of the two bands exhibit distinctly higher reactivity. As mentioned above, multiply coordinated OH groups (O from ZrO_2) absorb in this region. Obviously only this type of OH group is able to undergo H/D exchange reactions with D_2 at room temperature. The selectivity of the exchange reaction is confirmed by investigations on CVD ZrO_2 material degassed at 400 °C.[28] This sample shows a much higher intensity in the OH stretching region, especially in the high frequency range of the band $(OH)_{II}$. All the same, only the OH groups in the low frequency region, show H/D isotope exchange reactions.[28]

During the H/D isotope exchange reaction a linear correlation is observed for the growth of the OD bands at 2771 and 2692 cm^{-1} as well as for the depletion of the OH bands at 3757 and 3650 cm^{-1}. Therefore, the reaction mechanism and the kinetics seem to be the same for the two types of surface centres. The two OH bands $(OH)_I$ and $(OH)_{II}$ originate from OH groups containing differently coordinated O^{2-}. Trigonally coordinated O^{2-} anions only exist in the monoclinic structure. Therefore, OH groups giving rise to the band $(OH)_I$ [intensity loss at 3757 cm^{-1} and intensity gain at 2771 cm^{-1} in the OD stretching region (Fig. 7)] must be located at monoclinic surface domains. On the other hand, both monoclinic and tetragonal ZrO_2 contain tetrahedrally coordinated O^{2-} anions which give rise to the band $(OH)_{II}$. The linear correlated intensity increase of the bands at 2692 cm^{-1} $[(OD)_I]$ and 2771 cm^{-1} $[(OD)_{II}]$ then must lead to the conclusion that the reactive surface sites are located exclusively on *one* surface phase, namely the monoclinic one. The OH absorption at 3650 cm^{-1} must, therefore, as the band at 3757 cm^{-1}, be attributed to OH groups located on monoclinic surface domains. This nicely fits with the assignment derived above related to the influence of thermal pretreatment on the OH distribution.

OH groups on commercially available ZrO_2 do not permit H/D isotope exchange reaction at room temperature to any significant extent (Fig. 8). This cannot be explained by a smaller value of the specific surface area as compared to CVD ZrO_2: the spectra in Fig. 8 are normalized to the same specific surface area. According to transmission electron micrographs the commercial material has more regular crystallite surfaces and, therefore, likely contains less low-coordinated surface sites than the CVD sample. In addition, the production of the commercial sample favours the formation of tetragonal surface domains (see above). Thus the absence of reactivity of surface OH groups on commercial ZrO_2 with respect to the H/D

isotope exchange may conclusively be interpreted in terms of a shortage of both low-coordinated surface sites and monoclinic surface domains. This explanation is supported by the reaction of CO_2 with surface OH groups on ZrO_2.[29] This occurs exclusively on monoclinic and not on tetragonal surface domains.

Conclusions

The major issue of the present investigation is that ZrO_2 produced by CVD in our laboratories exhibits, by one to two orders of magnitude, more low-coordinated sites per unit specific surface area as compared to commercially available material. For catalytic applications of ZrO_2 the monoclinic surface domains play a particularly important role. The low-coordinated surface oxygen anions on these microplanes are extremely reactive and give rise to OH groups which selectively permit H/D isotope exchange already at room temperature. Therefore, the development of ZrO_2 catalysts should not only be focused on the enrichment of low-coordinated surface sites. The stabilization of monoclinic surface domains which are metastable for ZrO_2 particles with a diameter of <100 Å[20] is equally important. In addition, the role of anion as well as cation defects in chemical processes on the surface of highly dispersed ZrO_2 has, so far, not yet been elucidated in detail. Preliminary studies in our own laboratories clearly show that they should not be neglected.

Acknowledgements

We thank Dr M. Giersig, Dr D. Su and Mrs U. Bloeck from the HMI, Berlin, for taking the transmission electron micrographs. Thanks are also due to Degussa AG (Hanau, Germany) for providing ZrO_2 samples (2094E and Et57).

References

1 T. Yamagushi, *Catal. Today*, 1994, **20**, 199.
2 M. Y. He and J. G. Ekerdt, *J. Catal.*, 1984, **87**, 381.
3 K. Domen, J. Kondo, K. Maruya and T. Onishi, *Catal. Lett.*, 1992, **12**, 127.
4 Y. Nakano, T. Yamaguchi and K. Tanabe, *J. Catal.*, 1983, **80**, 307.
5 G. K. Chuah, S. Jaenicke, S. A. Cheong and K. S. Chan, *Appl. Catal. A: Gen.*, 1996, **145**, 267.
6 C. M. Foster, G. R. Bai, J. C. Parker and M. N. Ali, *J. Mater. Res.*, 1993, **8**, 1977.
7 M. Inoue, H. Kominami and T. Inui, *Appl. Catal. A*, 1995, **121,** L1.
8 T. Okubo and H. Nagamoto, *J. Mater. Sci.*, 1995, **30**, 749.
9 M. L. Rojas-Cervantes, R. M. Martin-Aranda, A. J. Lopez-Peinado and J. de D. Lopez-Gonzales, *J. Mater. Sci.*, 1994, **29**, 3743.
10 H. Toraya, *J. Am. Ceram. Soc.*, 1989, **72**, 662.
11 R. Suyama, T. Asida and S. Kume, *J. Am. Ceram. Soc.*, 1985, **68**, 314.
12 S. Brunauer, P. H. Emmett and E. Teller, *J. Am. Chem. Soc.*, 1938, **60**, 309.
13 P. Hoffmann and E. Knözinger, *Surf. Sci.*, 1987, **188**, 181.
14 P. Scherrer, *Göttinger Nachr.*, 1918, **2**, 98.
15 B. E. Warren, *X-Ray diffraction*, Addison-Wesley, Reading, 1969.
16 G. Caglioti, A. Paoletti and F. P. Ricci, *Nucl. Instrum.*, 1958, **3**, 223.
17 W. W. Barker, F. P. Bailey and W. Garrett, *J. Solid State Chem.*, 1973, **7**, 448.
18 R. C. Garvie, *J. Phys. Chem.*, 1965, **69**, 1238.
19 R. C. Garvie and M. F. Goss, *J. Mater. Sci.*, 1986, **21**, 1253.
20 R. C. Garvie, *J. Phys. Chem.*, 1978, **82**, 218.
21 W. Vogel, B. Tesche and W. Schulze, *Chem. Phys.*, 1983, **74**, 137.
22 R. Nitsche, M. Winterer, M. Croft and H. Hahn, *Nucl. Instrum. Methods B*, 1995, **97**, 127.
23 D. K. Smith and H. W. Newkirk, *Acta Crystallogr.*, 1965, **18**, 983.
24 J. D. McCoullough and K. N. Trueblood, *Acta Crystallogr.*, 1959, **12**, 507.
25 K.-H. Jacob, E. Knözinger and S. Benfer, *J. Mater. Chem.*, 1993, **3**, 651.
26 G. Teufer, *Acta Crystallogr.*, 1962, **15**, 1187.
27 E. Knözinger, K.-H. Jacob, S. Singh and P. Hofmann, *Surf. Sci.*, 1993, **290**, 388.
28 S. Benfer, P. Hofmann and E. Knözinger, *J. Mol. Struct.*, 1997, **410–411**, 115.
29 K.-H. Jacob, Dissertation, Siegen, 1992.

Paper 8/09164A